

Increased Asian Sulfate Aerosol Emissions Remarkably Enhance Sahel Summer Precipitation

J. Guo, Y. Liu

To be published in "Earth's Future"

November 2024

Environmental and Climate Sciences Department
Brookhaven National Laboratory

U.S. Department of Energy

USDOE Office of Science (SC), Biological and Environmental Research (BER)

Notice: This manuscript has been authored by employees of Brookhaven Science Associates, LLC under Contract No. DE-SC0012704 with the U.S. Department of Energy. The publisher by accepting the manuscript for publication acknowledges that the United States Government retains a non-exclusive, paid-up, irrevocable, world-wide license to publish or reproduce the published form of this manuscript, or allow others to do so, for United States Government purposes.

DISCLAIMER

This report was prepared as an account of work sponsored by an agency of the United States Government. Neither the United States Government nor any agency thereof, nor any of their employees, nor any of their contractors, subcontractors, or their employees, makes any warranty, express or implied, or assumes any legal liability or responsibility for the accuracy, completeness, or any third party's use or the results of such use of any information, apparatus, product, or process disclosed, or represents that its use would not infringe privately owned rights. Reference herein to any specific commercial product, process, or service by trade name, trademark, manufacturer, or otherwise, does not necessarily constitute or imply its endorsement, recommendation, or favoring by the United States Government or any agency thereof or its contractors or subcontractors. The views and opinions of authors expressed herein do not necessarily state or reflect those of the United States Government or any agency thereof.

Earth's Future



RESEARCH ARTICLE

10.1029/2024EF004745

Increased Asian Sulfate Aerosol Emissions Remarkably Enhance Sahel Summer Precipitation

Key Points:

- Increased Asian and reduced European sulfate aerosol emissions both enhance Sahel summer precipitation
- Asian anthropogenic aerosols partly drive the recent recovery in Sahel precipitation amounts
- The Sahel drought will be intensified likely due to the reductions in Asian aerosol emissions in SSP2-45

Jianing Guo^{1,2}, Xiaoning Xie^{1,3} , Gunnar Myhre⁴ , Drew Shindell⁵ , Alf Kirkevåg⁶, Trond Iversen⁶ , Bjørn H. Samset⁴ , Zhengguo Shi^{1,7} , Xinzhou Li¹ , Hui Sun¹ , Xiaodong Liu^{1,2} , and Yangang Liu⁸ 

¹SKLLQG, Institute of Earth Environment, Chinese Academy of Sciences, Xi'an, China, ²College of Earth and Planetary Sciences, University of Chinese Academy of Sciences, Beijing, China, ³CAS Center for Excellence in Quaternary Science and Global Change, Xi'an, China, ⁴CICERO - Center for International Climate Research, Oslo, Norway, ⁵Nicholas School of the Environment, Duke University, Durham, NC, USA, ⁶Norwegian Meteorological Institute, Oslo, Norway, ⁷Institute of Global Environmental Change, Xi'an Jiaotong University, Xi'an, China, ⁸Environmental and Climate Sciences Department, Brookhaven National Laboratory, Upton, NY, USA

Supporting Information:

Supporting Information may be found in the online version of this article.

Correspondence to:

X. Xie,
xnxie@ieecas.cn

Citation:

Guo, J., Xie, X., Myhre, G., Shindell, D., Kirkevåg, A., Iversen, T., et al. (2024). Increased Asian sulfate aerosol emissions remarkably enhance Sahel summer precipitation. *Earth's Future*, 12, e2024EF004745. <https://doi.org/10.1029/2024EF004745>

Received 29 MAR 2024

Accepted 30 OCT 2024

Abstract Observational evidence shows that Sahel summer precipitation has experienced a considerable increase since the 1980s, coinciding with significant diverging trends of increased sulfate emissions in Asia and decreased emissions in Europe (dipole pattern of aerosols between Asia and Europe). The decrease in European sulfate aerosols has substantial effects on the Sahel summer precipitation increase, but the corresponding effect of increased Asian sulfate is unknown. Multi-model simulations in the Precipitation Driver and Response Model Intercomparison Project (PDRMIP) show, compared to decreased European aerosols, that increased Asian aerosols similarly enhance the Sahel summer precipitation but with different large-scale atmospheric circulation changes. Further analysis of the Sixth Coupled Model Intercomparison Project (CMIP6) simulations under historical attribution and various emission scenarios reinforces the results about the climate impacts of anthropogenic aerosols and suggests that in future scenarios with strong international cooperation and rapid climate mitigations (SSP2-45), the Sahel drought will be intensified likely due to the decline in Asian aerosol emissions. Our results suggest that Asian anthropogenic aerosols are likely a non-negligible driver of the recent recovery in Sahel precipitation amounts.

Plain Language Summary Due to the widespread influences of Sahel summer rainfall on local people's livelihoods, sustainable resource management, ecosystem, and food security, its dynamic evolution and driving factors are a severe socio-economic concern. Owing to urbanization and industrialization, anthropogenic aerosol emissions over Asia have rapidly increased since the 1980s, but the climate impact of Asian aerosol emissions on local precipitation is unknown. Using the multi-model simulations in the Precipitation Driver and Response Model Intercomparison Project (PDRMIP), we show that increased Asian and reduced European sulfate aerosol emissions both enhance Sahel summer precipitation through different large-scale atmospheric circulation changes. Here, we highlight the long-range impact of Asian anthropogenic air pollutants on the recent recovery of Sahel precipitation and propose the Sahel drought will be intensified likely due to the decline in Asian aerosol emissions in future scenarios with strong international cooperation and rapid climate mitigations.

1. Introduction

The Sahel region is one of the most vulnerable regions to climate change, which experienced multi-decadal variations in regional precipitation during the twentieth century. Severe drought in the 1970s and 1980s seriously impacted local people's livelihoods, sustainable resource management, ecosystem, and food security (Epule et al., 2014; Gonzalez et al., 2012; Nyariki & Wiggins, 1997). The Sahel summer precipitation associated with the West African Monsoon (WAM) has recovered considerably since the 1980s (Biasutti, 2016, 2019; Gianini, 2015; Sanogo et al., 2015).

Many previous studies suggest that the recovery of Sahel precipitation is associated with global warming induced by human-produced greenhouse gases (GHGs) through various physical mechanisms (Dong & Sutton, 2015; Fontaine et al., 2011; Haarsma et al., 2005; Panthou et al., 2014; Sanogo et al., 2015; Schneider, Bischoff, & Haug, 2014; Schneider, & Becker et al., 2014; Sylla et al., 2015; Taylor et al., 2017). Both observations and model

© 2024. The Author(s).

This is an open access article under the terms of the [Creative Commons Attribution License](https://creativecommons.org/licenses/by/4.0/), which permits use, distribution and reproduction in any medium, provided the original work is properly cited.

simulations indicate a greater warming of the North African continent compared to the surrounding oceans and a significant decrease in continental sea-level pressure under global warming, which enhances the meridional temperature and pressure gradients, thereby inducing a stronger WAM circulation and increased summer precipitation in the Sahel (Dong & Sutton, 2015; Haarsma et al., 2005). The northward shift of the Inter-Tropical Convergence Zone (ITCZ) is associated with the GHG-induced tropical expansion mainly through warming the tropical upper troposphere, expanding the monsoon zone, and enhancing the summer precipitation in the Sahel (Fontaine et al., 2011; Schneider, Bischoff, & Haug, 2014; Schneider, & Becker et al., 2014). In thermodynamic effects, an increase in atmospheric moisture enhanced hydrological cycle due to global warming has contributed positively to precipitation changes and significantly increased the frequency and intensity of extreme precipitation in the Sahel (Kitoh et al., 2013; Panthou et al., 2014; Sanogo et al., 2015; Sylla et al., 2015; Taylor et al., 2017; Wang, Jin, & Liu, 2020; Wang, Le, et al., 2020). In addition, a number of studies on the causes of the Sahelian rainfall variability ranging from decades to centuries focused on the role of sea surface temperatures (SSTs, Bader et al., 2003; Folland et al., 1986; Giannini et al., 2003; Giannini, 2015; Held et al., 2005; Hagos & Cook, 2008; Shanahan et al., 2009). Several studies have linked the decadal increase in Sahel rainfall with the positive AMO phase (Diatta & Fink, 2014; Knight et al., 2006; Mohino et al., 2024; Monerie et al., 2019; O'Reilly et al., 2017; Ting et al., 2009; Zhang & Delworth, 2006), driven by the ITCZ northward shift (Knight et al., 2006). The long-lasting drought periods spanning decades to centuries are also linked to the AMO over the last three millennia based on the reconstructed African monsoon (Shanahan et al., 2009). Using an atmospheric general circulation model, Mohino et al. (2011) propose that low-frequency variations of Sahel rainfall were interpreted as the competition of the AMO, the tropical SST warming induced by global warming, and inter-decadal Pacific Oscillation, they further attribute 50% of the SST-driven Sahel drought to a shift to the negative AMO phase in the 1980s, while the contribution of global warming was 10%.

As one of the dominant contributors to climate forcing (Baker et al., 2015; Kasoar et al., 2018), anthropogenic aerosols affect global and regional climate by perturbing Earth's energy budget through scattering solar radiation and interacting with clouds by changing cloud microphysical properties (Booth et al., 2012; Jia et al., 2021; Rotstayn & Lohmann, 2002; Shindell & Faluvegi, 2009; Wang, Jin, & Liu, 2020; Wang, Le, et al., 2020). Sulfate aerosols scatter solar radiation and cool the Earth's surface, while black carbon (BC) absorbs shortwave radiation and warms the atmosphere, and both may have opposite effects on atmospheric circulation and regional precipitation (Bond et al., 2013; Myhre et al., 2013; Ramanathan et al., 2008). Several studies have examined the response of Sahel summer precipitation to sulfate aerosol variations in the uniform increase or reduction over the latitudinal band and hemispheric scale (Ackerley et al., 2011; Baker et al., 2015; Hwang et al., 2013; Jacobson et al., 2020; Kristjansson et al., 2005; Monerie et al., 2023; Rotstayn & Lohmann, 2002; Shindell et al., 2012). However, emissions of anthropogenic aerosols over Europe and Asia are spatially diverging since the 1980s, exhibiting a dipole pattern characterized by an increase in Asian sulfate aerosols and a decrease in European sulfate aerosols (Aas et al., 2019; Lu et al., 2011; Manktelow et al., 2007; Smith et al., 2011; Vestreng et al., 2007). The Asian anthropogenic sulfate increase (AASI) results in a weakening of the Asian monsoonal circulation and a reduction in summer precipitation in northern China and South Asia (Bollasina et al., 2011; Dong et al., 2016; Giorgi et al., 2003; Huang et al., 2007; Ramanathan et al., 2005; Xie et al., 2016, 2020), but an increase in precipitation over Central Asia through the equatorward shift of the Asian Westerly Jet Stream (Xie et al., 2022). In addition, the European anthropogenic sulfate decrease (EASD) affects local precipitation through changing surface temperature over land and the downstream ocean (Tang et al., 2018; Westervelt et al., 2018). More recently, a number of studies have indicated that the increase in the interhemispheric temperature gradient caused by the reduction of aerosols in Europe and North America and the associated meridional movement of the ITCZ has a remote influence on summer precipitation in the Sahel (Hirasawa et al., 2022; Monerie et al., 2023; Undorf et al., 2018; Westervelt et al., 2017, 2018). It remains unclear whether or not the increase in Asian sulfate aerosol has a long-range impact on summer precipitation in the Sahel.

To address the aforementioned questions, here we investigate the influence of EASD and AASI on Sahel summer precipitation based on global climate model (GCM) simulations. We analyze the multi-model simulation results of the Precipitation Driver and Response Model Intercomparison Project (PDRMIP) to identify the response of Sahel precipitation to EASD and AASI and underlying physical mechanisms. We further analyze historical simulations and future projections under different emission scenarios in the Sixth Coupled Model Intercomparison Project (CMIP6) to provide robust evidence from these sensitivity results in PDRMIP.

Table 1
Descriptions of PDRMIP Models Used in the Study

Model	Version	Resolution	Ocean setup	Aerosol emissions	Indirect effects of sulfate included
GISS-E2-R	E2-R	2° × 2.5°, 40 levels	Coupled ocean	Fixed concentrations	No indirect effects
HadGEM3	3	1.875° × 1.25°, 85 levels	Coupled ocean	Fixed concentrations	All indirect effects
IPSL-CM5A	5A	3.75° × 1.875°, 39 levels	Coupled ocean	Fixed concentrations	First indirect effect
MIROC-SPRINTARS	5.9.0	1.4° × 1.4°, 40 levels	Coupled ocean	Emissions	All indirect effects
NCAR-CESM1-CAM4	1.0.3	2.5° × 1.9°, 26 levels	Slab ocean	Fixed concentrations	No indirect effects
NCAR-CESM1-CAM5	1.1.2	2.5° × 1.9°, 30 levels	Coupled ocean	Emissions	All indirect effects
NorESM1	1-M	2.5° × 1.9°, 26 levels	Coupled ocean	Fixed concentrations	All indirect effects

2. Data and Methods

2.1. Observation and Reanalysis Data

In this study, we use four observational precipitation data sets which are widely used in climate variability studies. The Version 2.3 of the Global Precipitation Climatology Project (GPCP) monthly data set covers both land and ocean with a horizontal resolution of 2.5° × 2.5° from 1979 to the present (Adler et al., 2018). The Climatic Research Unit (CRU) version 4.05 provides a monthly land precipitation data set with a horizontal resolution of 0.5° × 0.5° from 1901 to 2020 (Harris et al., 2020). The monthly precipitation of the Global Precipitation Climatology Center (GPCC) version 2020 with a horizontal resolution of 0.25° × 0.25° from 1891 to 2019 is calculated from global station data (Schneider, Bischoff, & Haug, 2014; Schneider, & Becker et al., 2014; Schneider et al., 2020). The University of Delaware (UDEL) version 4.01 monthly land precipitation data set spans 1901–2014 with a horizontal resolution of 0.5° × 0.5° (Willmott & Matsuura, 2001). The observed wind field data is obtained from the National Centers for Environmental Prediction (NCEP)–Department of Energy (DOE), which is used to validate simulations of wind fields in the PDRMIP. The wind field horizontal resolution and the study period are the same as the GPCP data set. Compared to NCEP–the National Center for Atmospheric Research (NCAR), NCEP–DOE fixes known processing problems and uses improved forecast models and data assimilation systems, which is an updated version of NCEP–NCAR reanalysis (Kanamitsu et al., 2002). The reanalysis data set used in the analyses of Eurasian sulfate aerosol changes is monthly sulfate AOD from the Modern-Era Retrospective Analysis for Research and Applications, Version 2 (MERRA-2) Reanalysis. MERRA-2 includes aerosols in the reanalysis for the first time and provides an AOD data set from 1980 to the present, which is widely used in the study of aerosol properties (Gelaro et al., 2017; Randles et al., 2017). The monthly sulfate AOD data used in this study has a horizontal resolution of 2.5° × 2.5° and spans the period 1980–2020.

2.2. PDRMIP Simulations

The multi-model simulation results of the Precipitation Driver and Response Model Intercomparison Project (PDRMIP) are used to help us understand the precipitation responses to Asian and European aerosol forcings (Andrews et al., 2021; Liu et al., 2018; Myhre et al., 2017, 2022). Seven models used in this study have simulated one baseline (Base) experiment based on the condition of anthropogenic and natural climate forcing in 2000 and regional sulfate in Asia and Europe perturbation experiments with a tenfold increase in sulfate concentrations (some models increase in sulfate aerosol emissions) compared to the Base experiment for Asia (Sulx10Asia) and Europe (Sulx10Eur) respectively (see Table 1 for model descriptions; Liu et al., 2018; Myhre et al., 2017, 2022). Sulx10Asia-Base represents the climate response of Asian anthropogenic sulfate increase (AASI) and Base-Sulx10Eur represents the climate response of European anthropogenic sulfate decrease (EASD). Sulx10Asia-Sulx10Eur indicates the climate response of the combination of sulfate aerosol changes in Asia and Europe (AASI + EASD). The corresponding descriptions can be summarized as follows,

$$\text{AASI} = \text{Sulx10Asia} - \text{Base} \quad (1)$$

$$\text{EASD} = \text{Base} - \text{Sulx10Eur} \quad (2)$$

$$\text{AASI} + \text{EASD} = \text{Sulx10Asia} - \text{Sulx10Eur} \quad (3)$$

In addition, these models have also performed the Asia black carbon (BC) perturbation experiments with a tenfold increase in BC concentrations or emissions over Asia compared to the Base experiment (BCx10Asia; Mythe et al., 2022; Liu et al., 2018). Each experiment has performed a coupled ocean simulation (only NCAR-CESM1-CAM4 performed a slab ocean simulation) and a fixed-SST simulation. For the coupled or slab ocean simulation, each model runs for at least 100 years and selects the last 50 years for analysis. For the fixed-SST simulation, each model runs for at least 15 years and selects the last 10 years for analysis. These run lengths were chosen for analyses to ensure that the model reaches approximate equilibration and to encompass internal annual and decadal variabilities (Samset et al., 2016). According to the definition of ERF mentioned above, only the fixed-SST simulation is utilized to analyze the ERF under Asian and European sulfate perturbation in this study (Forster et al., 2016; Hansen et al., 2005; Myhre et al., 2013; Smith et al., 2020). Since each model has a different resolution, the horizontal resolution is bilinearly interpolated to $2.5^\circ \times 2.5^\circ$, and the vertical coordinates are converted to a 17-level pressure coordinate system.

2.3. CMIP6 Simulations

In addition to the numerical simulations about regional aerosol changes in PDRMIP (such as Asian and European aerosols), we further analyze the relative contributions of different external drivers to the Sahel summer precipitation increase using the Detection and Attribution Model Intercomparison Project (DAMIP) in CMIP6 (Gillett et al., 2016; see Text S1 in Supporting Information S1 for models and experiment descriptions). To further check the impact of future climate change on the Sahel summer precipitation, we use the multi-model simulated data from the Scenario Model Intercomparison Project (ScenarioMIP, O'Neill et al., 2016) in CMIP6. Fifteen models are selected to calculate the Sahel summer precipitation future trends in 2021–2100 under SSP2-45, SSP3-70, and SSP5-85 conditions (Table S1 in Supporting Information S1). Four models with large ensembles in SSPs, including ACCESS-ESM1-5 (40 ensembles), CanESM5 (25 ensembles), MIROC6 (50 ensembles), and MPI-ESM1-2-LR (30 ensembles), used in this study, we average all ensembles of each model as one model in a multi-model ensemble. Due to the different model resolutions in CMIP6, the simulated data are bilinearly interpolated to a $2.5^\circ \times 2.5^\circ$ horizontal resolution. It should be noted that in the historical simulation, the historical period of 1979–2014 is derived from historical experiments in CMIP6, and that of 2015–2020 is directly derived from SSP2-45 in the ScenarioMIP for CMIP6.

3. Results

3.1. Observational Evidence Between Sahel Summer Precipitation and Aerosol Dipole Pattern

To examine the Sahel precipitation characteristics since the 1980s, four observational precipitation data sets with long-term time series from GPCP (1979–2020), CRU (1979–2020), UDEL (1979–2014), and GPCC (1979–2019) are used. Figure 1a shows that multi-year average monthly precipitation in the Sahel is mainly concentrated during the Northern Hemisphere (NH) summer (from June to September, labeled by JJAS), particularly during August. In North Africa, the large observed changes in summer precipitation are found over the Sahel region (Figure 1b and Figure S1 in Supporting Information S1), exhibiting a significant enhancement with most areas exceeding 1 mm day^{-1} per 100 years. The regionally averaged summer precipitation over the Sahel in Figure 1c exhibits linear trends of 1.67 mm day^{-1} per 100 years derived from the GPCP, 1.81 mm day^{-1} per 100 years derived from the CRU, 1.85 mm day^{-1} per 100 years derived from the UDEL, and 1.54 mm day^{-1} per 100 years derived from the GPCC. All the linear trends are statistically significant at the 99% confidence level. Although there are differences between the linear trends of the four observations, they all indicate a considerable increase in Sahel summer precipitation since the 1980s.

Over Asia and Europe, the trends of anthropogenic aerosol emissions have been diverging since the 1980s, showing a dipole pattern of spatial distribution (Aas et al., 2019; Manktelow et al., 2007; Smith et al., 2011). Owing to urbanization and industrialization with the absence of specific policy for clean air action, anthropogenic aerosol emissions in Asia have increased significantly in recent decades (especially in South and East Asia; Ohara et al., 2007; Lu et al., 2011). Meanwhile, the environmental issues in Europe have prompted the formulation of emission reduction strategies and the introduction of cleaner production technologies, resulting in a significant decline in European anthropogenic aerosol emissions (Crippa et al., 2016; Vestreng et al., 2007). Figure 1d shows the results based on the sulfate aerosol optical depth (AOD) from the Modern-Era Retrospective analysis for

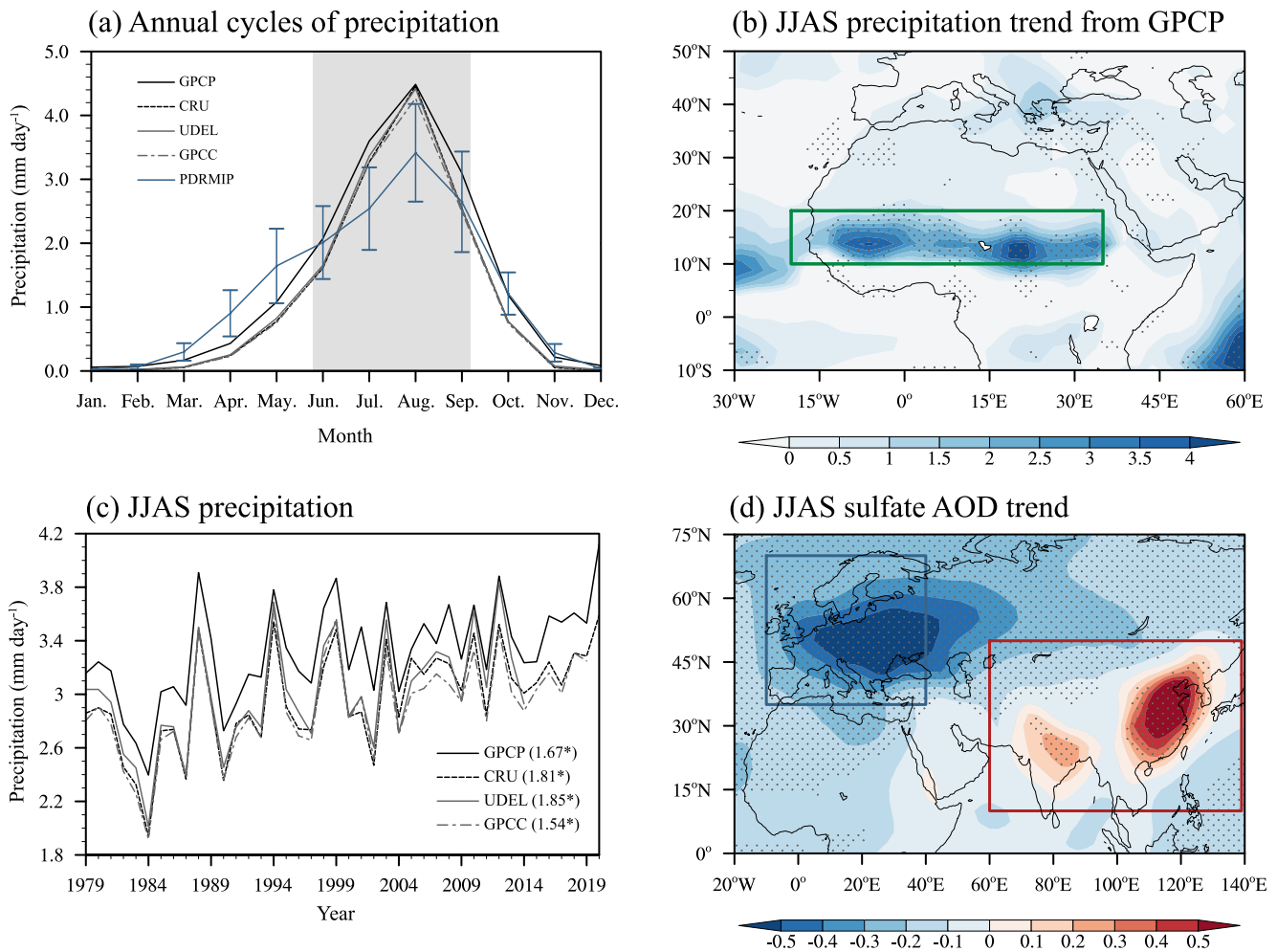


Figure 1. Relationships between Sahel precipitation and sulfate aerosols over Asia and Europe. (a) Annual cycle of Sahel (10°N–20°N, 20°W–35°E) precipitation (mm day^{-1}) derived from the GPCP (1979–2020), CRU (1979–2020), UDEL (1979–2014), GPCP (1979–2019) and Base experiments in PDRMIP. (b) Spatial distribution of precipitation trend (mm day^{-1} per 100 years) in summer (June–September, JJAS) from 1979 to 2020 derived from the GPCP. (c) Time series of JJAS precipitation over the Sahel, derived from the GPCP, CRU, UDEL, and GPCP. (d) Spatial pattern of Eurasian sulfate AOD trend (per 100 years) in JJAS during 1980–2020 from MERRA-2 Reanalysis. Error bars in (a) represent the multi-model ensemble standard deviation of PDRMIP. The thick green box in (b) marks the Sahel region. The numbers in the bracket in (c) represent the JJAS precipitation liner trend (mm day^{-1} per 100 years) and black stars represent that the trends are statistically significant at the 99% confidence level. The thick red and blue box in (d) indicates Asia (10°N–50°N, 60°E–140°E) and Europe regions (35°N–70°N, 10°W–40°E), respectively. Stippling in (b, d) represents $p < 0.05$ confidence level by a standard t -test.

Research and Applications version 2 (MERRA-2 Reanalysis, Gelaro et al., 2017), which shows a clear dipole pattern of decreased European but increased Asian sulfate AOD.

3.2. Sahel Precipitation Changes Induced by Aerosol Dipole Pattern

To examine the influence of EASD and AASI on the Sahel precipitation, we analyze the impact of European and Asian sulfate aerosol forcing on the Sahel precipitation using the PDRMIP sensitivity experiments and explore the potential physical mechanisms. Figure 2 shows the responses of Sahel summer precipitation to the dipole pattern in sulfate aerosol changes (increase in Asia but decrease in Europe). As shown in Figure 2, Sahel precipitation is significantly affected by EASD, AASI, and AASI + EASD. According to the monthly precipitation changes over the Sahel induced by EASD, Figure 2a shows a considerable increase in precipitation during JJAS with the maximum of 0.50 mm day^{-1} in August and the minimum of 0.10 mm day^{-1} in June. The seasonal average is $0.31 \pm 0.13 \text{ mm day}^{-1}$ for the multi-model mean in summer. Figure 2b shows the spatial distributions of EASD-induced changes in summer precipitation, indicating a considerable precipitation enhancement over the Sahel region, which is statistically significant. For AASI, a considerable increase in Sahel precipitation also

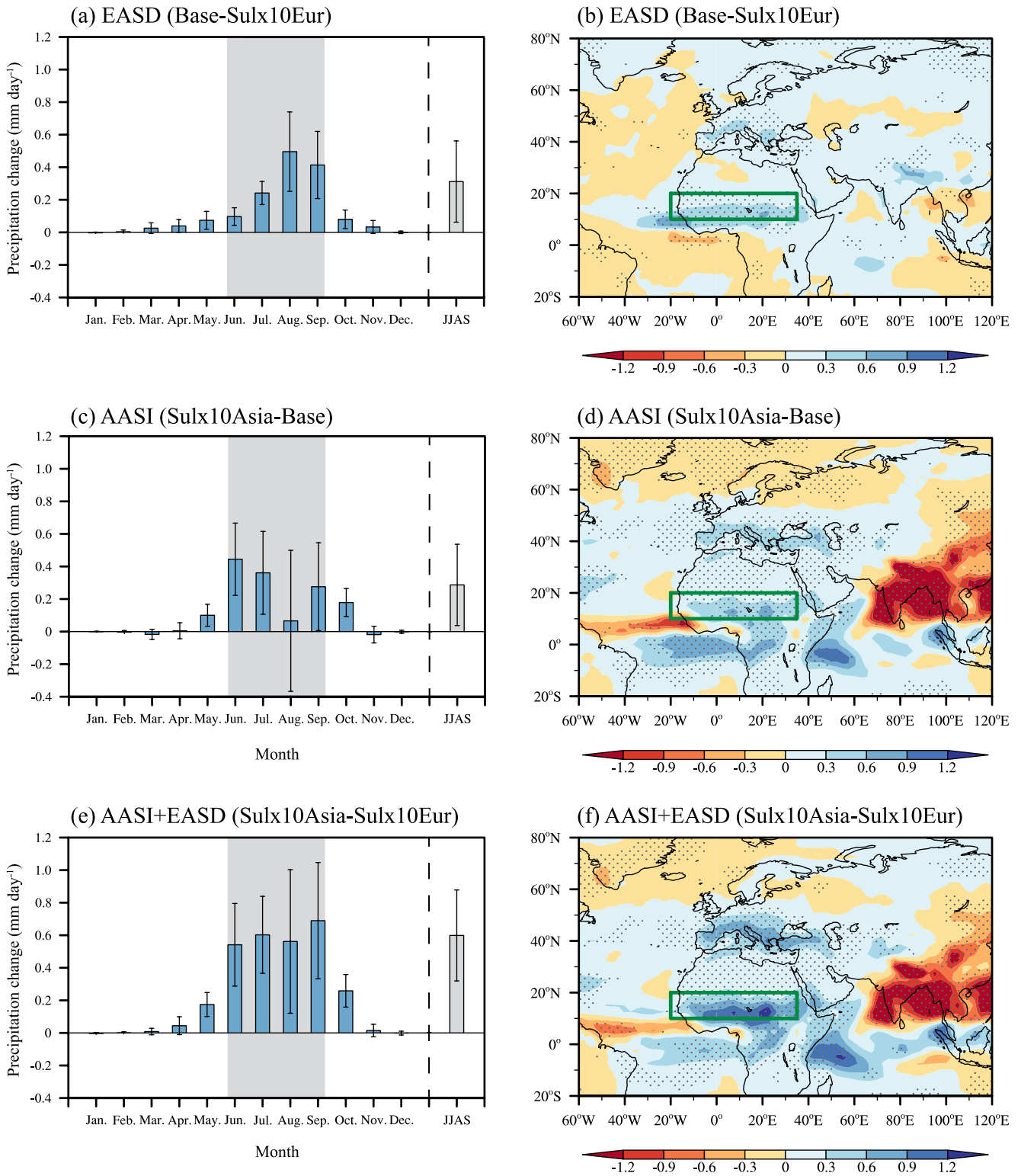


Figure 2. Sahel precipitation responses to sulfate aerosol dipole pattern in PDRMIP. (a) Monthly and JJAS average changes of Sahel precipitation (mm day^{-1}) induced by EASD (Base-Sulx10Eur), (c) AASI (Sulx10Asia-Base), and (e) AASI + EASD (Sulx10Asia-Sulx10Eur). Spatial distribution of changes in JJAS precipitation (mm day^{-1}) from (b) EASD, (d) AASI, and (f) AASI + EASD. Error bars in (a, c, e) represent the multi-model ensemble standard deviation of PDRMIP. The thick green box in (b, d, f) marks the Sahel region and the gray stippled regions indicate where the multi-model mean of the PDRMIP models is more than 1 standard deviation away from zero.

occurs in JJAS (Figure 2c), with the maximum of 0.44 mm day^{-1} in June and the minimum of 0.07 mm day^{-1} in August, and the summer seasonal average is $0.29 \pm 0.27 \text{ mm day}^{-1}$. The spatial distribution of summer precipitation change also indicates a significant increase over almost the whole Sahel region in Figure 2d. For the combined responses of Sahel precipitation to EASD and AASI, a stronger precipitation enhancement is revealed for JJAS (Figures 2e and 2f), and the precipitation changes in these months exceed 0.5 mm day^{-1} (Figure 2e). The seasonal average is $0.60 \pm 0.30 \text{ mm day}^{-1}$ for the multi-model mean in summer. These results show that EASD and AASI both enhance the Sahel summer precipitation, supporting the conclusion that the recent recovery in Sahel precipitation was partly driven by this dipole pattern of sulfate aerosols.

We use the circulation data from NCEP-DOE and precipitation from GPCP to compare the climatological spatial features of Base experiments in PDRMIP. As shown in Figure S2 in Supporting Information S1, the main spatial features of the precipitation, wind fields at different levels, and 200 hPa westerly jet stream during summer from the Base experiment are reproduced reasonably well, such as the distribution of WAM rain bands, the location of ITCZ, the center of African Easterly Jet (AEJ), and upper-level jet stream system. The multi-model mean also captures the annual cycle of Sahel precipitation, but underestimates Sahel summer precipitation, as seen in Figure 1a. Figure 2b shows that EASD significantly enhances summer precipitation over Europe and the western coast of the Indian Peninsula, consistent with previous studies (Shawki et al., 2018; Tang et al., 2018; Westervelt et al., 2018). AASI leads to a significant reduction in the summer precipitation over northern China and South Asia in Figure 2d, which is also consistent with previous studies (Bollasina et al., 2011; Dong et al., 2016; Giorgi et al., 2003; Huang et al., 2007; Ramanathan et al., 2005; Xie et al., 2016, 2020). Furthermore, this aerosol increase significantly enhances the summer precipitation over Central Asia, which was proposed by Xie et al. (2022).

Changes in Sahel summer precipitation mainly result from the adjustment of large-scale atmospheric circulations induced by the radiative forcing of Asian and European sulfate aerosol changes. The effective radiative forcing (ERF) is defined as the net radiative flux differences at the top of the atmosphere (TOA) between the Base and sensitivity experiments in fixed-SST simulations (Forster et al., 2016; Hansen et al., 2005; Myhre et al., 2013; Smith et al., 2020). As shown in Figure 3a, there is a large positive radiative forcing over Europe in the decreased European sulfate aerosol experiment. The positive ERF of sulfate aerosols leads to the significant warming of the troposphere from 1000 hPa to 200 hPa, with the greatest warming in the lower troposphere (Figure 3b). The spatial distribution of temperature changes at 850 hPa in the lower troposphere shows a significant increase in temperature (Figure 3c) over Europe and the Sahara Desert in combination with the warming over the Mediterranean and the North Atlantic (Figure S3a in Supporting Information S1), which induces a northward shift of the ITCZ and summer monsoon intensification (Fontaine et al., 2011; Shindell et al., 2012; Undorf et al., 2018; Westervelt et al., 2017, 2018). At the low-level troposphere, the regional warming results in a cyclonic flow pattern with an anomalous low-pressure center, and anomalous winds on the south side of the cyclonic circulation strengthen southwesterly winds in the African monsoon region (Figure 3d). The greater warming over the Sahara Desert enhances the sea-land thermal contrast between the Sahara Desert and the Atlantic Ocean and the temperature gradient with the equatorial regions of Africa, leading to the strengthening and northward movement (Figures 3e and 5) of the mid-tropospheric AEJ. The strengthening and northward movement of AEJ tends to favor the increases in zonal wind shear between 925 hPa and 600 hPa and the vertical upward motion over the Sahel (Figures 3g and 5, Grist & Nicholson, 2001; Taylor et al., 2017). The enhancement of the Tropical Easterly Jet (TEJ) is also associated with an intensification of vertical upward motion over the Sahel (Figures 3f and 3g; Grist & Nicholson, 2001; Fontaine et al., 2011). These changes all indicate the strengthening of the WAM system. Associated with the enhanced WAM, the vertically integrated moisture flux and convergence are also significantly increased over the Sahel region in Figure 3h and Figure S3b in Supporting Information S1 also with increased vertically integrated water vapor (Figure 3i). The enhanced WAM transports large amounts of water vapor from the tropical oceans to the Sahel with the intensified local vertical upward motion, leading to increased summer precipitation in the Sahel. Our results indicate that the EASD forcing enhances the Sahel summer precipitation by intensifying the WAM system.

Increased Asian sulfate aerosols induce a larger negative radiative forcing over Asia (Figure 4a), especially over eastern China and the Indian subcontinent. The negative ERF induced by AASI leads to tropospheric cooling at mid-latitudes about 20°N – 50°N (Figure 4b), where the cooling center (exceeding -1.6°) is at mid-high levels from 500 hPa to 200 hPa (Figure 4c). The mid-latitude cooling generates consequent changes in the meridional temperature gradient, with an increase in 20°N – 35°N and a decrease in 35°N – 50°N (Figure 4d). According to the

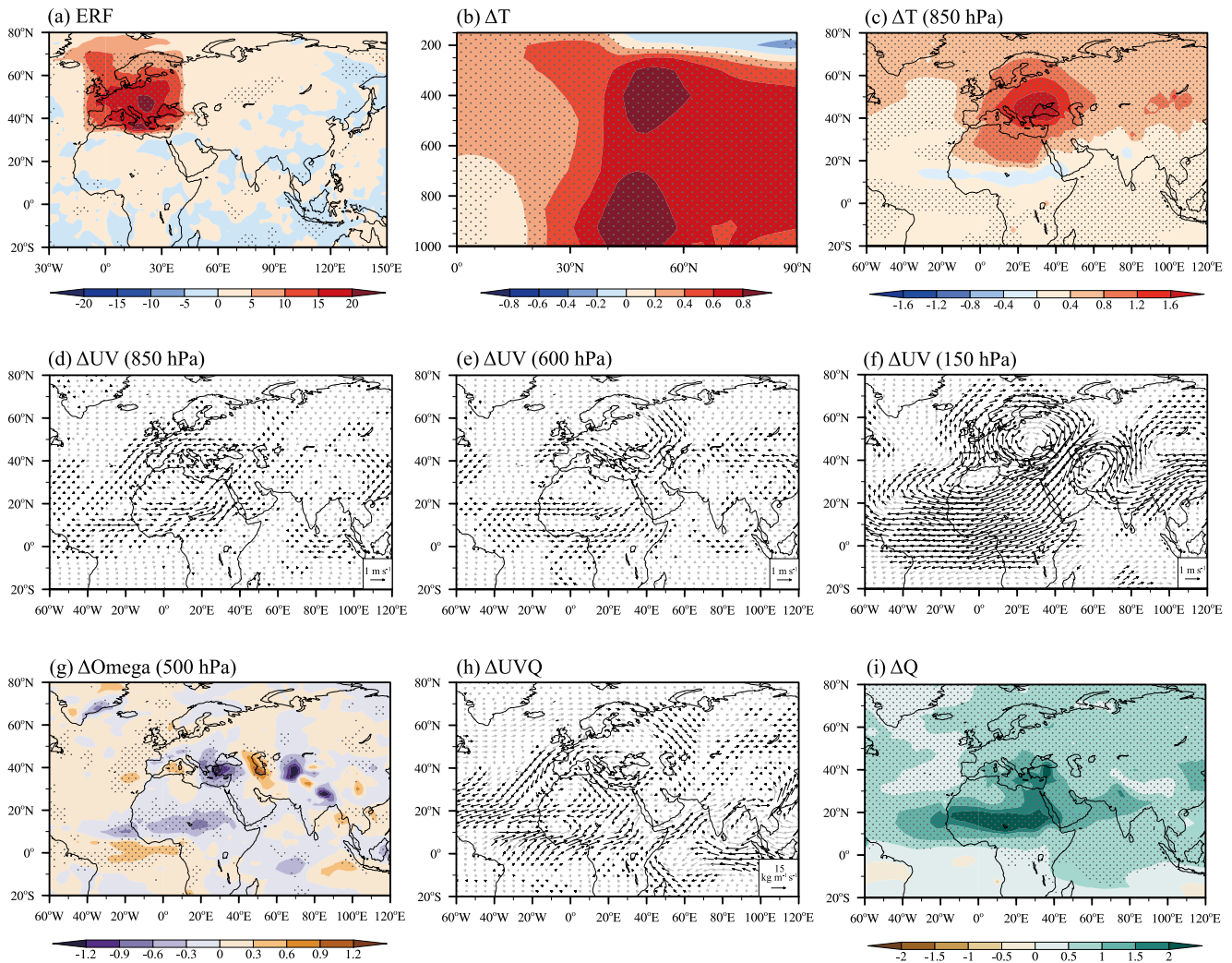


Figure 3. Multi-model mean anomalies induced by decreased European sulfate aerosols in PDRMIP. (a) JJAS effective radiative forcing (ERF, W m^{-2}). (b) Changes in JJAS zonal mean (10°W – 140°E) temperature (ΔT , $^{\circ}\text{C}$) and (c) 850 hPa temperature (ΔT , $^{\circ}\text{C}$). (d) Changes in JJAS wind field (ΔUV , m s^{-1}) at 850 hPa, (e) 600 hPa, and (f) 150 hPa. (g) Changes in JJAS 500 hPa vertical velocity (ΔOmega , $10^{-2} \text{ Pa s}^{-1}$), (h) vertically integrated (surface–300 hPa) moisture flux (ΔUVQ , $\text{kg m}^{-1} \text{ s}^{-1}$), and (i) vertically integrated (surface–300 hPa) water vapor (ΔQ , kg m^{-2}). The gray stippled regions in (a, b, c, g, i) and black arrows in (d, e, f, h) indicate where the multi-model mean of the PDRMIP models is more than 1 standard deviation away from zero.

thermal wind principle, the change of zonal wind is proportional to the temperature gradient (Mann et al., 2018). The changes in the temperature gradient lead to a weakening of the mid-latitude westerly wind and a strengthening of the low-latitude westerly wind at 200 hPa (Figure 4e), indicating a southward shift of the westerly jet stream. Enhanced low-latitude westerlies also occur at 500–850 hPa levels over the eastern Atlantic and North Africa (Figures 4f and 4g) associated with the southward shift in the westerly jet. Furthermore, the increased zonal winds (Figure 5) in cooperation with the changes of the vertically integrated moisture flux (Figure 4h) and vertically integrated water vapor (Figure 4i, with an average across the Sahel of 0.24 kg m^{-2} in Table S2 in Supporting Information S1) indicate a considerable enhancement in water vapor transport to the Sahel from the Atlantic Ocean through enhancing the westerlies. It is noted that the enhanced westerlies at low latitudes favor moisture transportation from the eastern Atlantic to the Sahel (Pu & Cook, 2010), which consequently enhances the Sahel summer precipitation. Additionally, as shown in Figure 5, the atmospheric circulation indices related to the WAM are characterized by a weakening of the AEJ and a weakening of the easterly shear, which are opposite to that of EASD. The changes in the latitude of the AEJ show that all models indicate a northward shift of the AEJ induced by EASD, supporting the strengthening of WAM. For AASI, the changes in the latitude of AEJ have large uncertainty and are insignificant, strongly dependent on models (positive for 5 models and negative for 2 models).

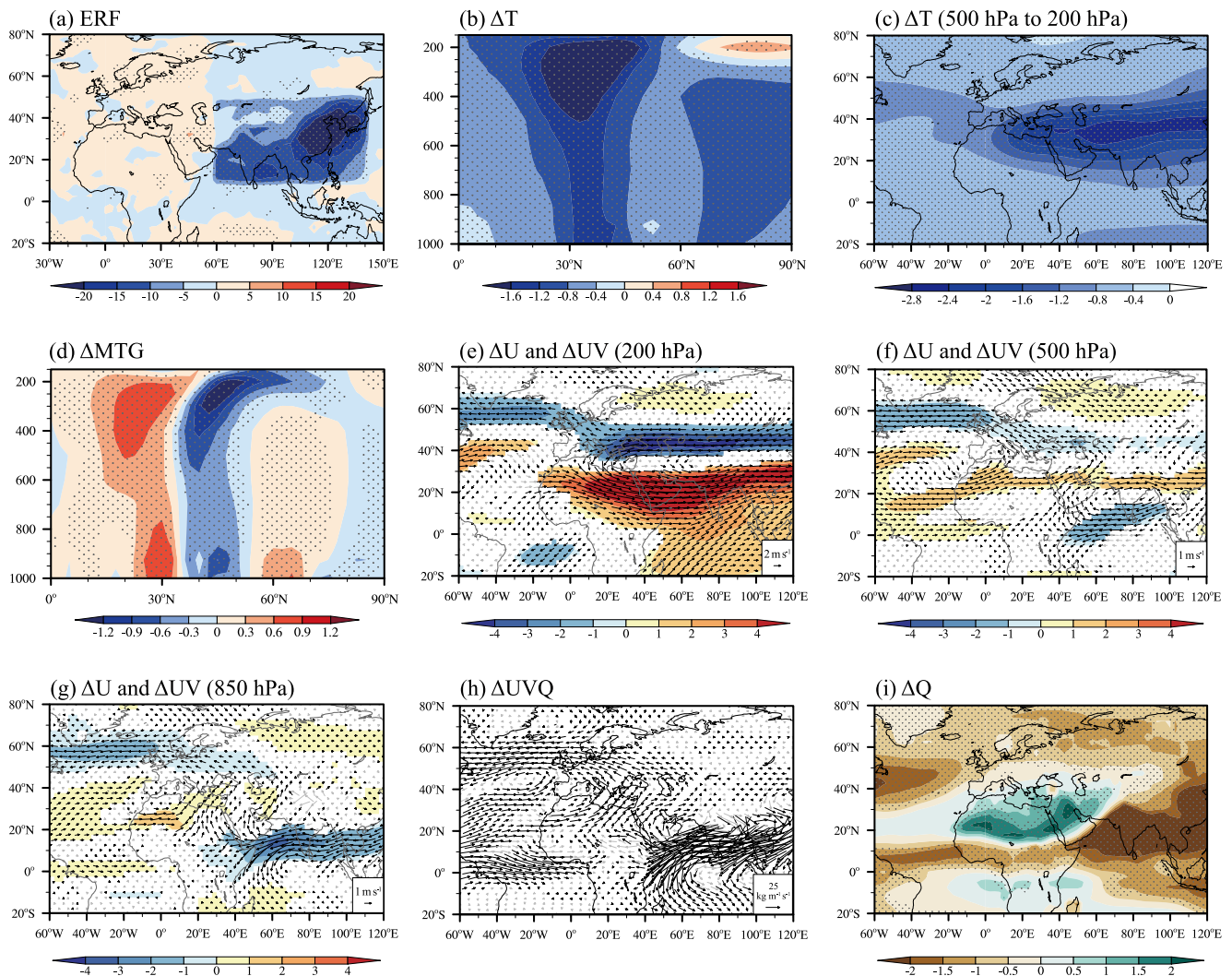


Figure 4. Multi-model mean anomalies induced by increased Asian sulfate aerosols in PDRMIP. (a) JJAS effective radiative forcing (ERF, W m^{-2}). (b) Changes in JJAS zonal mean (10°W – 140°E) temperature (ΔT , $^{\circ}\text{C}$). (c) temperature (ΔT , $^{\circ}\text{C}$) from 500 hPa to 200 hPa, and (d) zonal mean (10°W – 140°E) temperature gradient (ΔMTG , $10^{-3} \text{ }^{\circ}\text{C km}^{-1}$). (e) Variations of wind field (ΔUV , vector, m s^{-1}) and zonal wind (ΔU , shaded, m s^{-1}) at 200 hPa, (f) 500 hPa, and (g) 850 hPa in JJAS. (h) Changes in JJAS vertically integrated (surface–300 hPa) moisture flux (ΔUVQ , $\text{kg m}^{-1} \text{ s}^{-1}$) and (i) vertically integrated (surface–300 hPa) water vapor (ΔQ , kg m^{-2}). The gray stippled regions in (a, b, c, d, i), black arrows in (e, f, g, h), and the colored in (e, f, g) contour maps indicate where the multi-model mean of the PDRMIP models is more than 1 standard deviation away from zero.

The changes indicate that AASI enhances Sahel summer precipitation through strengthening low-latitude westerlies induced by the southward shift of the westerly jet stream, instead of intensifying the WAM.

3.3. The Influence of Black Carbon on Sahel Precipitation

In contrast to scattering sulfate aerosols, black carbon (BC) absorbs the short-wave radiation and warms the atmosphere, likely leading to opposite effects on atmospheric circulation and regional precipitation (Myhre et al., 2017; Ramanathan & Carmichael, 2008; Samset et al., 2016; Xie et al., 2022; Zhao et al., 2020). Asia, as one of the major BC emission regions in the world, has shown a significant increase in BC emissions in recent decades (Bond et al., 2013; Li et al., 2016). We further investigate the Sahel summer precipitation response to the increased Asian BC effects, diagnosed as the difference between BCx10Asia and BASE experiments in PDRMIP. The BC perturbation shows a significant positive ERF over Asia (Figure S4a in Supporting Information S1) and a strong warming around the mid-latitudes (Figure S4b in Supporting Information S1). Increased Asian BC aerosols induce a poleward shift of the westerly jet stream (Figure S4c in Supporting Information S1) and the weakened low-latitude westerlies over North Africa (Figures S4d and S4e in Supporting Information S1) through

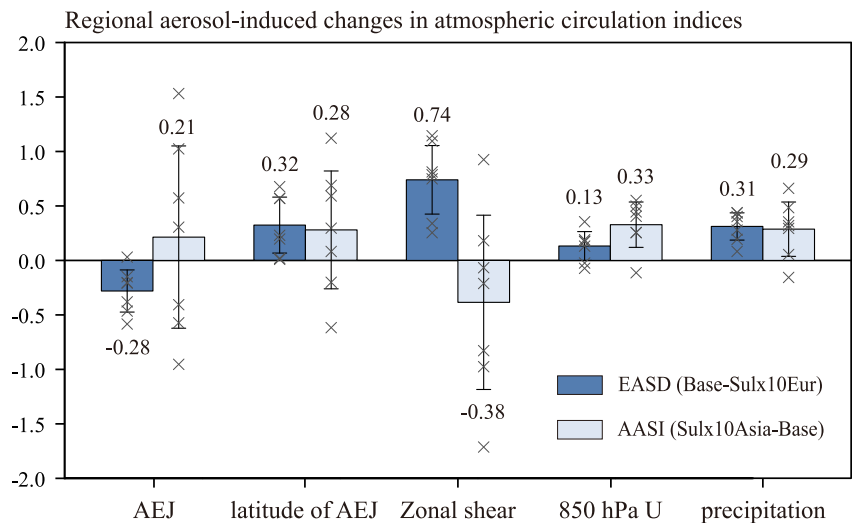


Figure 5. Responses of atmospheric circulation indices related to the Sahel summer precipitation to regional aerosol changes in PDRMIP. Changes induced by EASD and AASI in the African Easterly Jet (AEJ, m s^{-1} , defined as the area-averaged zonal wind at 600 hPa over the Sahel), latitude of AEJ ($^{\circ}$ North, defined as the latitude of the maximum of the zonal mean easterly wind computed between 20°W and 35°E), vertical zonal wind shear (m s^{-1}) between 925 hPa and 600 hPa over the Sahel, zonal wind (U , m s^{-1}) at 850 hPa over the eastern Atlantic and western Africa (10°N – 30°N , 40°W – 10°E), and precipitation (mm day^{-1}) averaged over the Sahel. Crosses denote the results of each model. Bars represent ± 1 standard deviation of multi-model simulation results in PDRMIP.

warming the mid-latitude atmosphere, and thus reduce the Sahel summer precipitation insignificantly with an average across Sahel of $-0.09 \pm 0.14 \text{ mm day}^{-1}$ (Figure S4f in Supporting Information S1). These climate responses are opposite to the response to increased Asian sulfate aerosols (Figure 4) and partially offset the impact on Sahel precipitation of Asian sulfate aerosol perturbations.

3.4. Relative Contributions of Sahel Summer Precipitation Increase

To provide robust evidence from these sensitivity results in PDRMIP, we further analyze the relative contributions of different external drivers to the Sahel summer precipitation increase using the Detection and Attribution Model Intercomparison Project (DAMIP) in CMIP6 (Gillett et al., 2016). All-forcing historical simulation shows an increasing trend of the Sahel precipitation during 1979–2020 with a linear trend of 0.92 mm day^{-1} per 100 years (Figure S5a in Supporting Information S1). Further simulations with individual forcings in DAMIP indicate that anthropogenic aerosol change dominates the increasing trend (0.50 mm day^{-1} per 100 years), followed by GHGs with 0.33 mm day^{-1} per 100 years and nature aerosol change with 0.12 mm day^{-1} per 100 years (Figure S5a in Supporting Information S1). The DAMIP simulations clearly indicate that the dipole pattern of Asian and European aerosols has been a critical driver of the recent recovery in Sahel precipitation (Figure S5 in Supporting Information S1; Monerie et al., 2020). Note that the historical simulations significantly underestimate the increasing trend of JJAS precipitation over the Sahel in observations based on GPCP (1.67 mm day^{-1} per 100 years), CRU (1.81 mm day^{-1} per 100 years), UDEL (1.85 mm day^{-1} per 100 years), and GPCC (1.54 mm day^{-1} per 100 years). We further utilize two models for historical simulations with large ensembles, including CanESM5 (40 members) and MIROC6 (50 ensembles), to examine the contributions of internal and external forcings. The externally forced signal is calculated from all ensemble members mean and the internal variability is calculated from the deviation of each ensemble member from the ensemble mean (Wu et al., 2021). As shown in Figure S6 in Supporting Information S1, there are significant differences in precipitation trends induced by internal variability in both CanESM5 and MIROC6, implying the non-negligible influence of internal variability on the Sahel summer precipitation changes. It suggests that the underestimation of the multi-modal mean probably derives from the inability of the models to capture internal variability, such as the positive and negative phases of the AMO (Marvel et al., 2020). A large number of studies have attributed the decadal increase in Sahel rainfall to the changes in the AMO phase (Diatta & Fink, 2014; Folland et al., 1986; Knight et al., 2006; Mohino et al., 2011; O' Reilly et al., 2017; Rowell et al., 1995; Ting et al., 2009; Zhang & Delworth, 2006). The

uncertainty in the GCM parameterization of aerosol-radiative and aerosol-cloud processes can also lead to biases in precipitation simulations (Sato et al., 2018; Seinfeld et al., 2016). Note that the historical simulations in DAMIP suggest that the increasing trend of JJAS precipitation over the Sahel is mainly controlled by external forcings including GHGs and aerosols, the internal variability of AMO may partly contribute to the precipitation increase. The DAMIP simulation results support the recent recovery of precipitation since the 1980s mainly controlled by external forcing (Dong & Sutton, 2015).

3.5. Application to Future Projection of Sahel Summer Precipitation

To explore the implications of future climate changes, we further examine the future trends of Sahel summer precipitation in CMIP6 (Eyring et al., 2016). In comparison with Europe and North America, Asia will likely experience larger future changes in anthropogenic emissions of aerosols for the Shared Socioeconomic Pathways (SSPs) such as SSP2-45, SSP3-70, and SSP5-85 (O'Neill et al., 2017; Rao et al., 2017; Samset et al., 2019; Turnock et al., 2020), and exert stronger anthropogenic aerosol influence on future precipitation. In future scenarios with increasing GHG concentrations and reduced Asian aerosol emissions (SSP3-70 and SSP5-85), the Sahel summer precipitation displays a significant increasing trend with 0.27 mm day^{-1} per 100 years ($p < 0.01$) for SSP3-70 in Figure S7a in Supporting Information S1 and 0.20 mm day^{-1} per 100 years ($p < 0.01$) for SSP5-85 in Figure S7b in Supporting Information S1, which is much smaller than the historical trend of 1979–2020 (Figure S5a in Supporting Information S1). The less stringent regulation of aerosols and their precursors over Asia (Rao et al., 2017) may slightly inhibit Sahel summer precipitation, partially offsetting the precipitation increase induced by higher GHG concentrations. The “middle of the road” pathway of SSP2-45 corresponds to a significant decrease in Sahel summer precipitation ($-0.09 \text{ mm day}^{-1}$ per 100 years, $p < 0.05$, Figure S7c in Supporting Information S1), which mainly results from the decrease in the Asian aerosol emissions during 2020–2100. The result shows that the Sahel drought will be intensified likely due to the reductions in Asian aerosol emissions in future scenarios with strong international cooperation and rapid climate mitigations.

4. Conclusion and Discussion

The observations show that after an extreme drought, NH summer precipitation in the Sahel has considerably recovered since the 1980s. Inspection of the idealized sensitivity experiments from multi-model simulations in PDRMIP reveals that the concurrent Asian anthropogenic sulfate increase (AASI) and the European anthropogenic sulfate decrease (EASD) both enhance summer precipitation in the Sahel. Distinct circulation patterns including WAM and westerlies on the Sahel precipitation are induced by Asian and European sulfate aerosols, respectively. The PDRMIP simulations show that the decrease in sulfate aerosols over Europe intensifies the WAM and increases regional precipitation through warming in the lower troposphere over Europe and the Sahara Desert and shifting ITCZ northwards, which is consistent with previous studies (Fontaine et al., 2011; Shindell et al., 2012; Undorf et al., 2018; Westervelt et al., 2017, 2018). Here, we suggest, instead of intensifying the WAM, that the increase in Asian sulfate aerosols strengthens the low-latitude westerlies induced by the southward shift of the westerly jet stream to increase the Sahel precipitation. The attribution analysis in DAMIP shows that the change in anthropogenic aerosol concentration levels is an important external forcing of Sahel summer precipitation increase, compared with GHGs and natural forcing, suggesting that the recent rainfall recovery in the Sahel was partly caused by this dipole pattern of Eurasian sulfate aerosols. Furthermore, the future projections in CMIP6 suggest that the Sahel drought will be intensified likely due to the decline in Asian aerosol emissions in future scenarios with the limitation of greenhouse gas emissions through strong international cooperation and rapid climate mitigations (SSP2-45).

Although our results suggest that the opposite changes of sulfate aerosols between Asia and Europe lead to adjustments in atmospheric circulations and thus might have contributed to the recovery of Sahel precipitation in recent decades, anthropogenic aerosols over other regions such as North America and Africa also alter the Sahel precipitation. In combination with European sulfate aerosols, the reduction in North American sulfate aerosols enhances the Sahel summer precipitation by strengthening the interhemispheric temperature gradient (Haywood et al., 2016; Monerie et al., 2023; Westervelt et al., 2018). Local changes in African anthropogenic aerosol emissions also significantly affect WAM and the Sahel summer precipitation (Hirasawa et al., 2022; Lund et al., 2019; Shindell et al., 2023; Wells et al., 2023), and the large uncertainty in aerosol emissions over northern Africa probably contributes to large uncertainty in estimated changes in the Sahel precipitation in the near future (Lund et al., 2019; Monerie et al., 2023; Shindell et al., 2023).

Data Availability Statement

The data that support the findings of this study are freely available. The monthly sulfate AOD of MERRA-2 can be found at <https://disc.gsfc.nasa.gov/datasets?project=MERRA-2> (Gelaro et al., 2017). The GPCP version 2.3 monthly mean precipitation data set is available at <https://psl.noaa.gov/data/gridded/data.gpcp.html> (Adler et al., 2018). The CRU version 4.05 monthly land precipitation data set is available at https://crudata.uea.ac.uk/cru/data/hrg/cru_ts_4.05/cruts.2103051243.v4.05/pre/ (Harris et al., 2020). The monthly precipitation of the GPCP version 2020 is available at https://downloads.psl.noaa.gov/Datasets/gpcp/full_v2020/precip.mon.total.0.25x0.25.v2020.nc (Schneider et al., 2020). The UDEL version 4.01 monthly land precipitation data set is available at <https://downloads.psl.noaa.gov/Datasets/udel.airt.precip/v401/> (Willmott & Matsuura, 2001). NCEP-DOE Reanalysis 2 wind field data are available at <https://psl.noaa.gov/data/gridded/data.ncep.reanalysis2.html> (Kanamitsu et al., 2002). The PDRMIP data set of numerical simulations can be accessed online at https://doi.org/10.26050/WDCC/PDRMIP_2012-2021 (Andrews et al., 2021; Myhre et al., 2022). All the CMIP6 simulation data sets are downloaded through the web interface <https://aims2.llnl.gov/search/cmip6/>. In this manuscript, the NCAR Command Language (NCL) version 6.6.2 was utilized for data processing and visualization, and this software is available from <https://www.ncl.ucar.edu/>.

Acknowledgments

This research has been supported by the National Key R&D Program of China (2023YFF0804804) and the Strategic Priority Research Program of the Chinese Academy of Sciences (XDB40030100). X.N.X. is supported by the National Natural Science Foundation of China (42175059) and the CAS “Light of West China” program (XAB2019A02). Z.G.S. also acknowledges the support of Youth Innovation Promotion Association CAS (Y2022101) and the Natural Science Basic Research Program of Shaanxi Province (2022JC-17). X.Z.L. is supported by the CIRP Open Fund of Radiation Protection Laboratories (ZFYFSHJ-2023001). Y.L. was supported by the US Department of Energy's Atmospheric System Research (ASR) program.

References

- Aas, W., Mortier, A., Bowersox, V., Cherian, R., Faluvegi, G., Fagerli, H., et al. (2019). Global and regional trends of atmospheric sulfur. *Scientific Reports*, 9(1), 953. <https://doi.org/10.1038/s41598-018-37304-0>
- Ackerley, D., Booth, B. B. B., Knight, S. H. E., Highwood, E. J., Frame, D. J., Allen, M. R., & Rowell, D. P. (2011). Sensitivity of twentieth-century Sahel rainfall to sulfate aerosol and CO₂ forcing. *Journal of Climate*, 24(19), 4999–5014. <https://doi.org/10.1175/JCLI-D-11-00019.1>
- Adler, R. F., Sapiano, M. R. P., Huffman, G. J., Wang, J. J., Gu, G., Bolvin, D., et al. (2018). The Global Precipitation Climatology Project (GPCP) monthly analysis (new version 2.3) and a review of 2017 global precipitation [Dataset]. *Atmosphere*, 9(4), 138. <https://doi.org/10.3390/atmos9040138>
- Andrews, T., Boucher, O., Fläschner, D., Kasoar, M., Kharin, V. V., Kirkevåg, A., et al. (2021). Precipitation driver response model inter-comparison project data sets 2013–2021 [Dataset]. *World Data Center for Climate (WDCC) at DKRZ*. https://doi.org/10.26050/WDCC/PDRMIP_2012-2021
- Bader, J., & Latif, M. (2003). The impact of decadal-scale Indian Ocean sea surface temperature anomalies on Sahelian rainfall and the North Atlantic Oscillation. *Geophysical Research Letters*, 30(22), 2169. <https://doi.org/10.1029/2003GL018426>
- Baker, L. H., Collins, W. J., Olivie, D. J. L., Cherian, R., Hodnebrog, Ø., Myhre, G., & Quaas, J. (2015). Climate responses to anthropogenic emissions of short-lived climate pollutants. *Atmospheric Chemistry and Physics*, 15(14), 8201–8216. <https://doi.org/10.5194/acp-15-8201-2015>
- Bernell, E., Zhang, Q., Chafik, L., & Körnich, H. (2018). Representation of multidecadal Sahel rainfall variability in 20th century reanalyses. *Scientific Reports*, 8(1), 10937. <https://doi.org/10.1038/s41598-018-29217-9>
- Biasutti, M. (2013). Forced Sahel rainfall trends in the CMIP5 archive. *Journal of Geophysical Research: Atmospheres*, 118(4), 1613–1623. <https://doi.org/10.1002/jgrd.50206>
- Biasutti, M. (2016). What brings rain to the Sahel? *Nature Climate Change*, 6(10), 897–898. <https://doi.org/10.1038/nclimate3080>
- Biasutti, M. (2019). Rainfall trends in the African sahel: Characteristics, processes, and causes. *Wiley Interdisciplinary Reviews: Climate Change*, 10(4), e591. <https://doi.org/10.1002/wcc.591>
- Bollasina, M. A., Ming, Y., & Ramaswamy, V. (2011). Anthropogenic aerosols and the weakening of the South Asian summer monsoon. *Science*, 334(6055), 502–505. <https://doi.org/10.1126/science.1204994>
- Bond, T. C., Doherty, S. J., Fahey, D. W., Forster, P. M., Bernsten, T., DeAngelo, B. J., et al. (2013). Bounding the role of black carbon in the climate system: A scientific assessment. *Journal of Geophysical Research: Atmospheres*, 118(11), 5380–5552. <https://doi.org/10.1002/jgrd.50171>
- Booth, B. B. B., Dunstone, N. J., Halloran, P. R., Andrews, T., & Bellouin, N. (2012). Aerosols implicated as a prime driver of twentieth-century North Atlantic climate variability. *Nature*, 485(7399), 534. <https://doi.org/10.1038/nature11138>
- Crippa, M., Janssens-Maenhout, G., Dentener, F., Guizzardi, D., Sindelarova, K., Muntean, M., et al. (2016). Forty years of improvements in European air quality: Regional policy-industry interactions with global impacts. *Atmospheric Chemistry and Physics*, 16(6), 3825–3841. <https://doi.org/10.5194/acp-16-3825-2016>
- Diatta, S., & Fink, A. H. (2014). Statistical relationship between remote climate indices and West African monsoon variability. *International Journal of Climatology*, 34(12), 3348–3367. <https://doi.org/10.1002/joc.3912>
- Dong, B., & Sutton, R. (2015). Dominant role of greenhouse-gas forcing in the recovery of Sahel rainfall. *Nature Climate Change*, 5(8), 757–760. <https://doi.org/10.1038/nclimate2664>
- Dong, B., Sutton, R. T., Highwood, E. J., & Wilcox, L. J. (2016). Preferred response of the East Asian summer monsoon to local and non-local anthropogenic Sulphur dioxide emissions. *Climate Dynamics*, 46(5–6), 1733–1751. <https://doi.org/10.1007/s00382-015-2671-5>
- Dong, B., Sutton, R. T., Shaffrey, L., & Harvey, B. (2022). Recent decadal weakening of the summer Eurasian westerly jet attributable to anthropogenic aerosol emissions. *Nature Communications*, 13(1), 1148. <https://doi.org/10.1038/s41467-022-28816-5>
- Epule, E. T., Peng, C., Lepage, L., & Chen, Z. (2014). The causes, effects and challenges of Sahelian droughts: A critical review. *Regional Environmental Change*, 14(1), 145–156. <https://doi.org/10.1007/s10113-013-0473-z>
- Eyring, V., Bony, S., Meehl, G. A., Senior, C. A., Stevens, B., Stouffer, R. J., & Taylor, K. E. (2016). Overview of the coupled model inter-comparison project phase 6 (CMIP6) experimental design and organization. *Geoscientific Model Development*, 9(5), 1937–1958. <https://doi.org/10.5194/gmd-9-1937-2016>
- Folland, C. K., Palmer, T. N., & Parker, D. E. (1986). Sahel rainfall and worldwide sea temperatures, 1901–85. *Nature*, 320(6063), 602–607. <https://doi.org/10.1038/320602a0>

- Fontaine, B., Roucou, P., Gaetani, M., & Marteau, R. (2011). Recent changes in precipitation, ITCZ convection and northern tropical circulation over North Africa (1979-2007). *International Journal of Climatology*, 31(5), 633–648. <https://doi.org/10.1002/joc.2108>
- Forster, P. M., Richardson, T., Maycock, A. C., Smith, C. J., Samset, B. H., Myhre, G., et al. (2016). Recommendations for diagnosing effective radiative forcing from climate models for CMIP6. *Journal of Geophysical Research: Atmospheres*, 121(20), 12460–12475. <https://doi.org/10.1002/2016JD025320>
- Gelaro, R., McCarty, W., Suárez, M. J., Todling, R., Molod, A., Takacs, L., et al. (2017). The modern-era retrospective analysis for research and applications, version 2 (MERRA-2) [Dataset]. *Journal of Climate*, 30(14), 5419–5454. <https://doi.org/10.1175/JCLI-D-16-0758.1>
- Giannini, A. (2015). Climate change comes to the Sahel. *Nature Climate Change*, 5(8), 720–721. <https://doi.org/10.1038/nclimate2739>
- Giannini, A., Saravanan, R., & Chang, P. (2003). Oceanic forcing of Sahel rainfall on interannual to interdecadal time scales. *Science*, 302(5647), 1027–1030. <https://doi.org/10.1126/science.1089357>
- Gillett, N. P., Shiogama, H., Funke, B., Hegerl, G., Knutti, R., Matthes, K., et al. (2016). The detection and attribution model intercomparison project (DAMIP v1. 0) contribution to CMIP6. *Geoscientific Model Development*, 9(10), 3685–3697. <https://doi.org/10.5194/gmd-9-3685-2016>
- Giorgi, F., Bi, X., & Qian, Y. (2003). Indirect vs. direct effects of anthropogenic sulfate on the climate of East Asia as simulated with a regional coupled climate-chemistry/aerosol model. *Climatic Change*, 58(3), 345–376. <https://doi.org/10.1023/A:1023946010350>
- Gonzalez, P., Tucker, C. J., & Sy, H. (2012). Tree density and species decline in the African Sahel attributable to climate. *Journal of Arid Environments*, 78, 55–64. <https://doi.org/10.1016/j.jaridenv.2011.11.001>
- Grist, J. P., & Nicholson, S. E. (2001). A study of the dynamic factors influencing the rainfall variability in the West African Sahel. *Journal of Climate*, 14(7), 1337–1359. [https://doi.org/10.1175/1520-0442\(2001\)014<1337:ASOTDF>2.0.CO;2](https://doi.org/10.1175/1520-0442(2001)014<1337:ASOTDF>2.0.CO;2)
- Haarsma, R. J., Selten, F. M., Weber, S. L., & Kliphuis, M. (2005). Sahel rainfall variability and response to greenhouse warming. *Geophysical Research Letters*, 32(17), L17702. <https://doi.org/10.1029/2005GL023232>
- Hagos, S. M., & Cook, K. H. (2008). Ocean warming and late-twentieth-century Sahel drought and recovery. *Journal of Climate*, 21(15), 3797–3814. <https://doi.org/10.1175/2008JCLI2055.1>
- Hansen, J., Sato, M. K. I., Ruedy, R., Nazarenko, L., Lacis, A., Schmidt, G. A., et al. (2005). Efficacy of climate forcing's. *Journal of Geophysical Research*, 110(D18), D18104. <https://doi.org/10.1029/2005JD005776>
- Harris, I., Osborn, T. J., Jones, P., & Lister, D. (2020). Version 4 of the CRU TS monthly high-resolution gridded multivariate climate dataset [Dataset]. *Scientific Data*, 7(1), 109. <https://doi.org/10.1038/s41597-020-0453-3>
- Haywood, J. M., Jones, A., Bellouin, N., & Stephenson, D. (2013). Asymmetric forcing from stratospheric aerosols impacts Sahelian rainfall. *Nature Climate Change*, 3(7), 660–665. <https://doi.org/10.1038/nclimate1857>
- Haywood, J. M., Jones, A., Dunstone, N., Milton, S., Vellinga, M., Bodas-Salcedo, A., et al. (2016). The impact of equilibrating hemispheric albedos on tropical performance in the HadGEM2-ES coupled climate model. *Geophysical Research Letters*, 43(1), 395–403. <https://doi.org/10.1002/2015GL066903>
- Held, I. M., Delworth, T. L., Lu, J., Findell, K. U., & Knutson, T. R. (2005). Simulation of Sahel drought in the 20th and 21st centuries. *Proceedings of the National Academy of Sciences*, 102(50), 17891–17896. <https://doi.org/10.1073/pnas.0509057102>
- Hirasawa, H., Kushner, P. J., Sigmond, M., Fyfe, J., & Deser, C. (2022). Evolving Sahel rainfall response to anthropogenic aerosols driven by shifting regional oceanic and emission influences. *Journal of Climate*, 35(11), 3181–3193. <https://doi.org/10.1175/JCLI-D-21-0795.1>
- Huang, Y., Chameides, W. L., & Dickinson, R. E. (2007). Direct and indirect effects of anthropogenic aerosols on regional precipitation over East Asia. *Journal of Geophysical Research*, 112(D3), D03212. <https://doi.org/10.1029/2006JD007114>
- Hwang, Y. T., Frierson, D. M., & Kang, S. M. (2013). Anthropogenic sulfate aerosol and the southward shift of tropical precipitation in the late 20th century. *Geophysical Research Letters*, 40(11), 2845–2850. <https://doi.org/10.1002/grl.50502>
- Jacobson, T. W., Yang, W., Vecchi, G. A., & Horowitz, L. W. (2020). Impact of volcanic aerosol hemispheric symmetry on Sahel rainfall. *Climate Dynamics*, 55(7), 1733–1758. <https://doi.org/10.1007/s00382-020-05347-7>
- Jia, H., Ma, X., Yu, F., & Quaas, J. (2021). Significant underestimation of radiative forcing by aerosol-cloud interactions derived from satellite-based methods. *Nature Communications*, 12(1), 3649. <https://doi.org/10.1038/s41467-021-23888-1>
- Kanamitsu, M., Ebisuzaki, W., Woollen, J., Yang, S. K., Hnilo, J. J., Fiorino, M., & Potter, G. L. (2002). Ncep-doe amip-ii reanalysis (r-2) [Dataset]. *Bulletin of the American Meteorological Society*, 83(11), 1631–1644. <https://doi.org/10.1175/BAMS-83-11-1631>
- Kasoar, M., Shawki, D., & Voulgarakis, A. (2018). Similar spatial patterns of global climate response to aerosols from different regions. *npj Climate and Atmospheric Science*, 1(1), 12. <https://doi.org/10.1038/s41612-018-0022-z>
- Kitoh, A., Endo, H., Krishna Kumar, K., Cavalcanti, I. F., Goswami, P., & Zhou, T. (2013). Monsoons in a changing world: A regional perspective in a global context. *Journal of Geophysical Research: Atmospheres*, 118(8), 3053–3065. <https://doi.org/10.1002/jgrd.50258>
- Knight, J. R., Folland, C. K., & Scaife, A. A. (2006). Climate impacts of the Atlantic multidecadal oscillation. *Geophysical Research Letters*, 33(17), L17706. <https://doi.org/10.1029/2006GL026242>
- Kristjánsson, J. E., Iversen, T., Kirkevåg, A., Seland, Ø., & Debernard, J. (2005). Response of the climate system to aerosol direct and indirect forcing: Role of cloud feedbacks. *Journal of Geophysical Research*, 110(D24), D24206. <https://doi.org/10.1029/2005JD006299>
- Li, Z., Lau, W. M., Ramanathan, V., Wu, G., Ding, Y., Manoj, M. G., et al. (2016). Aerosol and monsoon climate interactions over Asia. *Reviews of Geophysics*, 54(4), 866–929. <https://doi.org/10.1002/2015RG000500>
- Liu, L., Shawki, D., Voulgarakis, A., Kasoar, M., Samset, B. H., Myhre, G., et al. (2018). A PDRMIP multimodel study on the impacts of regional aerosol forcing's on global and regional precipitation. *Journal of Climate*, 31(11), 4429–4447. <https://doi.org/10.1175/JCLI-D-17-0439.1>
- Lu, Z., Zhang, Q., & Streets, D. G. (2011). Sulfur dioxide and primary carbonaceous aerosol emissions in China and India, 1996-2010. *Atmospheric Chemistry and Physics*, 11(18), 9839–9864. <https://doi.org/10.5194/acp-11-9839-2011>
- Lund, M. T., Myhre, G., & Samset, B. H. (2019). Anthropogenic aerosol forcing under the shared socioeconomic pathways. *Atmospheric Chemistry and Physics*, 19(22), 13827–13839. <https://doi.org/10.5194/acp-19-13827-2019>
- Manktelow, P. T., Mann, G. W., Carslaw, K. S., Spracklen, D. V., & Chipperfield, M. P. (2007). Regional and global trends in sulfate aerosol since the 1980s. *Geophysical Research Letters*, 34(14), L14803. <https://doi.org/10.1029/2006GL028668>
- Mann, M. E., Rahmstorf, S., Kornhuber, K., Steinman, B. A., Miller, S. K., Petri, S., & Coumou, D. (2018). Projected changes in persistent extreme summer weather events: The role of quasi-resonant amplification. *Science Advances*, 4(10), eaat3272. <https://doi.org/10.1126/sciadv.aat3272>
- Marvel, K., Biasutti, M., & Bonfils, C. (2020). Fingerprints of external forcing's on Sahel rainfall: Aerosols, greenhouse gases, and model-observation discrepancies. *Environmental Research Letters*, 15(8), 084023. <https://doi.org/10.1088/1748-9326/ab858e>
- Mohino, E., Janicot, S., & Bader, J. (2011). Sahel rainfall and decadal to multi-decadal sea surface temperature variability. *Climate Dynamics*, 37(3–4), 419–440. <https://doi.org/10.1007/s00382-010-0867-2>

- Mohino, E., Monerie, P. A., Mignot, J., Diakhaté, M., Donat, M., Roberts, C. D., & Doblas-Reyes, F. (2024). Impact of Atlantic multidecadal variability on rainfall intensity distribution and timing of the West African monsoon. *Earth System Dynamics*, *15*(1), 15–40. <https://doi.org/10.5194/esd-15-15-2024>
- Monerie, P. A., Dittus, A. J., Wilcox, L. J., & Turner, A. G. (2023). Uncertainty in simulating twentieth century West African precipitation trends: The role of anthropogenic aerosol emissions. *Earth's Future*, *11*(2), e2022EF002995. <https://doi.org/10.1029/2022EF002995>
- Monerie, P.-A., Robson, J., Dong, B., Hodson, D. L. R., & Klingaman, N. P. (2019). Effect of the Atlantic multidecadal variability on the global monsoon. *Geophysical Research Letters*, *46*(3), 1765–1775. <https://doi.org/10.1029/2018GL080903>
- Monerie, P. A., Wainwright, C. M., Sidibe, M., & Akinsanola, A. A. (2020). Model uncertainties in climate change impacts on Sahel precipitation in ensembles of CMIP5 and CMIP6 simulations. *Climate Dynamics*, *55*(5), 1385–1401. <https://doi.org/10.1007/s00382-020-05332-0>
- Myhre, G., Forster, P. M., Samset, B. H., Hodnebrog, Ø., Sillmann, J., Aalbergstjø, S. G., et al. (2017). PDRMIP: A precipitation driver and response model intercomparison project—Protocol and preliminary results. *Bulletin of the American Meteorological Society*, *98*(6), 1185–1198. <https://doi.org/10.1175/BAMS-D-16-0019.1>
- Myhre, G., Samset, B., Forster, P. M., Hodnebrog, Ø., Sandstad, M., Mohr, C. W., et al. (2022). Scientific data from precipitation driver response model intercomparison project [Dataset]. *Scientific Data*, *9*(1), 123. <https://doi.org/10.1038/s41597-022-01194-9>
- Myhre, G., Shindell, D., Bréon, F. M., Collins, W., Fuglestedt, J., Huang, J., et al. (2013). Climate change 2013: The physical science basis. In T. F. Stocker, D. Qin, G.-K. Plattner, M. Tignor, S. K. Allen, J. Doschung, et al. (Eds.), *Contribution of Working Group I to the Fifth Assessment Report of the Intergovernmental Panel on Climate Change*. Cambridge University Press.
- Nyariki, D. M., & Wiggins, S. (1997). Household food insecurity in sub-Saharan Africa: Lessons from Kenya. *British Food Journal*, *99*(7), 249–262. <https://doi.org/10.1108/00070709710179363>
- Ohara, T. A. H. K., Akimoto, H., Kurokawa, J. I., Horii, N., Yamaji, K., Yan, X., & Hayasaka, T. (2007). An Asian emission inventory of anthropogenic emission sources for the period 1980–2020. *Atmospheric Chemistry and Physics*, *7*(16), 4419–4444. <https://doi.org/10.5194/acp-7-4419-2007>
- O'Neill, B. C., Kriegler, E., Ebi, K. L., Kemp-Benedict, E., Riahi, K., Rothman, D. S., et al. (2017). The roads ahead: Narratives for shared socioeconomic pathways describing world futures in the 21st century. *Global Environmental Change*, *42*, 169–180. <https://doi.org/10.1016/j.gloenvcha.2015.01.004>
- O'Neill, B. C., Tebaldi, C., Van Vuuren, D. P., Eyring, V., Friedlingstein, P., Hurtt, G., et al. (2016). The scenario model intercomparison project (ScenarioMIP) for CMIP6. *Geoscientific Model Development*, *9*(9), 3461–3482. <https://doi.org/10.5194/gmd-9-3461-2016>
- O'Reilly, C. H., Woollings, T., & Zanna, L. (2017). The dynamical influence of the Atlantic multidecadal oscillation on continental climate. *Journal of Climate*, *30*(18), 7213–7230. <https://doi.org/10.1175/JCLI-D-16-0345.1>
- Panthou, G., Vischel, T., & Lebel, T. (2014). Recent trends in the regime of extreme rainfall in the Central Sahel. *International Journal of Climatology*, *34*(15), 3998–4006. <https://doi.org/10.1002/joc.3984>
- Pu, B., & Cook, K. H. (2010). Dynamics of the West African westerly jet. *Journal of Climate*, *23*(23), 6263–6276. <https://doi.org/10.1175/2010JCLI3648.1>
- Ramanathan, V., & Carmichael, G. (2008). Global and regional climate changes due to black carbon. *Nature Geoscience*, *1*(4), 221–227. <https://doi.org/10.1038/ngeo156>
- Ramanathan, V., Chung, C., Kim, D., Bettge, T., Buja, L., Kiehl, J. T., et al. (2005). Atmospheric brown clouds: Impacts on South Asian climate and hydrological cycle. *Proceedings of the National Academy of Sciences*, *102*(15), 5326–5333. <https://doi.org/10.1073/pnas.0500656102>
- Ramanathan, V., Crutzen, P. J., Kiehl, J. T., & Rosenfeld, D. (2001). Aerosols, climate, and the hydrological cycle. *Science*, *294*(5549), 2119–2124. <https://doi.org/10.1126/science.1064034>
- Randles, C. A., Da Silva, A. M., Buchard, V., Colarco, P. R., Darmenov, A., Govindaraju, R., et al. (2017). The MERRA-2 aerosol reanalysis, 1980 onward. Part I: System description and data assimilation evaluation. *Journal of Climate*, *30*(17), 6823–6850. <https://doi.org/10.1175/JCLI-D-16-0609.1>
- Rao, S., Klimont, Z., Smith, S. J., Van Dingenen, R., Dentener, F., Bouwman, L., et al. (2017). Future air pollution in the shared socio-economic pathways. *Global Environmental Change*, *42*, 346–358. <https://doi.org/10.1016/j.gloenvcha.2016.05.012>
- Rotstayn, L. D., & Lohmann, U. (2002). Tropical rainfall trends and the indirect aerosol effect. *Journal of Climate*, *15*(15), 2103–2116. [https://doi.org/10.1175/1520-0442\(2002\)015<2103:TRTATI>2.0.CO;2](https://doi.org/10.1175/1520-0442(2002)015<2103:TRTATI>2.0.CO;2)
- Rowell, D. P., Folland, C. K., Maskell, K., & Ward, M. N. (1995). Variability of summer rainfall over tropical North Africa (1906–92): Observations and modelling. *Quarterly Journal of the Royal Meteorological Society*, *121*(523), 669–704. <https://doi.org/10.1002/qj.49712152311>
- Samset, B. H., Lund, M. T., Bollasina, M., Myhre, G., & Wilcox, L. (2019). Emerging Asian aerosol patterns. *Nature Geoscience*, *12*(8), 582–584. <https://doi.org/10.1038/s41561-019-0424-5>
- Samset, B. H., Myhre, G., Forster, P. M., Hodnebrog, Ø., Andrews, T., Faluvegi, G., et al. (2016). Fast and slow precipitation responses to individual climate forcings: A PDRMIP multimodel study. *Geophysical Research Letters*, *43*(6), 2782–2791. <https://doi.org/10.1002/2016GL068064>
- Sanogo, S., Fink, A. H., Omotosho, J. A., Ba, A., Redl, R., & Ermert, V. (2015). Spatio-temporal characteristics of the recent rainfall recovery in West Africa. *International Journal of Climatology*, *35*(15), 4589–4605. <https://doi.org/10.1002/joc.4309>
- Sato, Y., Goto, D., Michibata, T., Suzuki, K., Takemura, T., Tomita, H., & Nakajima, T. (2018). Aerosol effects on cloud water amounts were successfully simulated by a global cloud-system resolving model. *Nature Communications*, *9*(1), 985. <https://doi.org/10.1038/s41467-018-03379-6>
- Schneider, T., Bischoff, T., & Haug, G. H. (2014). Migrations and dynamics of the intertropical convergence zone. *Nature*, *513*(7516), 45–53. <https://doi.org/10.1038/nature13636>
- Schneider, U., Becker, A., Finger, P., Meyer-Christoffer, A., Ziese, M., & Rudolf, B. (2014). GPCC's new land surface precipitation climatology based on quality-controlled in situ data and its role in quantifying the global water cycle. *Theoretical and Applied Climatology*, *115*(1–2), 15–40. <https://doi.org/10.1007/s00704-013-0860-x>
- Schneider, U., Becker, A., Finger, P., Rustemeier, E., & Ziese, M. (2020). GPCC full data monthly product version 2020 at 0.25°: Monthly land-surface precipitation from rain-gauges built on GTS-based and historical data [Dataset]. *GPCC*. https://doi.org/10.5676/DWD_GPCC/FD_M_V2020_025
- Seinfeld, J. H., Bretherton, C., Carslaw, K. S., Coe, H., DeMott, P. J., Dunlea, E. J., et al. (2016). Improving our fundamental understanding of the role of aerosol–cloud interactions in the climate system. *Proceedings of the National Academy of Sciences*, *113*(21), 5781–5790. <https://doi.org/10.1073/pnas.1514043113>
- Shanahan, T. M., Overpeck, J. T., Anchukaitis, K. J., Beck, J. W., Cole, J. E., Dettman, D. L., et al. (2009). Atlantic forcing of persistent drought in West Africa. *Science*, *324*(5925), 377–380. <https://doi.org/10.1126/science.1166352>

- Shawki, D., Voulgarakis, A., Chakraborty, A., Kasoar, M., & Srinivasan, J. (2018). The South Asian monsoon response to remote aerosols: Global and regional mechanisms. *Journal of Geophysical Research: Atmospheres*, *123*(20), 11585–11601. <https://doi.org/10.1029/2018JD028623>
- Shindell, D., & Faluvegi, G. (2009). Climate response to regional radiative forcing during the twentieth century. *Nature Geoscience*, *2*(4), 294–300. <https://doi.org/10.1038/ngeo473>
- Shindell, D., Parsons, L., Faluvegi, G., Hicks, K., Kuylenstierna, J., & Heaps, C. (2023). The important role of African emissions reductions in projected local rainfall changes. *npj Climate and Atmospheric Science*, *6*(1), 47. <https://doi.org/10.1038/s41612-023-00382-7>
- Shindell, D. T., Voulgarakis, A., Faluvegi, G., & Milly, G. (2012). Precipitation response to regional radiative forcing. *Atmospheric Chemistry and Physics*, *12*(15), 6969–6982. <https://doi.org/10.5194/acp-12-6969-2012>
- Smith, C. J., Kramer, R. J., Myhre, G., Alterskjær, K., Collins, W., Sima, A., et al. (2020). Effective radiative forcing and adjustments in CMIP6 models. *Atmospheric Chemistry and Physics*, *20*(16), 9591–9618. <https://doi.org/10.5194/acp-20-9591-2020>
- Smith, S. J., van Aardenne, J., Klimont, Z., Andres, R. J., Volke, A., & Delgado Arias, S. (2011). Anthropogenic sulfur dioxide emissions: 1850–2005. *Atmospheric Chemistry and Physics*, *11*(3), 1101–1116. <https://doi.org/10.5194/acp-11-1101-2011>
- Sylla, M. B., Giorgi, F., Pal, J. S., Gibba, P., Kebe, I., & Nikiema, M. (2015). Projected changes in the annual cycle of high-intensity precipitation events over West Africa for the late twenty-first century. *Journal of Climate*, *28*(16), 6475–6488. <https://doi.org/10.1175/JCLI-D-14-00854.1>
- Tang, T., Shindell, D., Samsset, B. H., Boucher, O., Forster, P. M., Hodnebrog, Ø., et al. (2018). Dynamical response of Mediterranean precipitation to greenhouse gases and aerosols. *Atmospheric Chemistry and Physics*, *18*(11), 8439–8452. <https://doi.org/10.5194/acp-18-8439-2018>
- Taylor, C. M., Belušić, D., Guichard, F., Parker, D. J., Vischel, T., Bock, O., et al. (2017). Frequency of extreme Sahelian storms tripled since 1982 in satellite observations. *Nature*, *544*(7651), 475–478. <https://doi.org/10.1038/nature22069>
- Ting, M., Kushnir, Y., Seager, R., & Li, C. (2009). Forced and internal twentieth-century SST trends in the North Atlantic. *Journal of Climate*, *22*(6), 1469–1481. <https://doi.org/10.1175/2008JCLI2561.1>
- Turnock, S. T., Allen, R. J., Andrews, M., Bauer, S. E., Deushi, M., Emmons, L., et al. (2020). Historical and future changes in air pollutants from CMIP6 models. *Atmospheric Chemistry and Physics*, *20*(23), 14547–14579. <https://doi.org/10.5194/acp-20-14547-2020>
- Undorf, S., Polson, D., Bollasina, M. A., Ming, Y., Schurer, A., & Hegerl, G. C. (2018). Detectable impact of local and remote anthropogenic aerosols on the 20th century changes of West African and South Asian monsoon precipitation. *Journal of Geophysical Research: Atmospheres*, *123*(10), 4871–4889. <https://doi.org/10.1029/2017JD027711>
- Vestreng, V., Myhre, G., Fagerli, H., Reis, S., & Tarrasón, L. (2007). Twenty-five years of continuous Sulphur dioxide emission reduction in Europe. *Atmospheric Chemistry and Physics*, *7*(13), 3663–3681. <https://doi.org/10.5194/acp-7-3663-2007>
- Wang, B., Jin, C., & Liu, J. (2020). Understanding future change of global monsoons projected by CMIP6 models. *Journal of Climate*, *33*(15), 6471–6489. <https://doi.org/10.1175/JCLI-D-19-0993.1>
- Wang, Y., Le, T., Chen, G., Yung, Y. L., Su, H., Seinfeld, J. H., & Jiang, J. H. (2020). Reduced European aerosol emissions suppress winter extremes over northern Eurasia. *Nature Climate Change*, *10*(3), 225–230. <https://doi.org/10.1038/s41558-020-0693-4>
- Wells, C. D., Kasoar, M., Bellouin, N., & Voulgarakis, A. (2023). Local and remote climate impacts of future African aerosol emissions. *Atmospheric Chemistry and Physics*, *23*(6), 3575–3593. <https://doi.org/10.5194/acp-23-3575-2023>
- Westervelt, D. M., Conley, A. J., Fiore, A. M., Lamarque, J. F., Shindell, D., Previdi, M., et al. (2017). Multimodel precipitation responses to removal of US sulfur dioxide emissions. *Journal of Geophysical Research: Atmospheres*, *122*(9), 5024–5038. <https://doi.org/10.1002/2017JD026756>
- Westervelt, D. M., Conley, A. J., Fiore, A. M., Lamarque, J. F., Shindell, D. T., Previdi, M., et al. (2018). Connecting regional aerosol emissions reductions to local and remote precipitation responses. *Atmospheric Chemistry and Physics*, *18*(16), 12461–12475. <https://doi.org/10.5194/acp-18-12461-2018>
- Willmott, C. J., & Matsuura, K. (2001). Terrestrial precipitation: 1900–2014 gridded monthly time series [Dataset]. https://climate.geog.udel.edu/html_pages/Global2014/README.GlobalTsP2014.html
- Wu, M., Zhou, T., Li, C., Li, H., Chen, X., Wu, B., et al. (2021). A very likely weakening of Pacific Walker Circulation in constrained near-future projections. *Nature Communications*, *12*(1), 6502. <https://doi.org/10.1038/s41467-021-26693-y>
- Xie, X., Myhre, G., Liu, X., Li, X., Shi, Z., Wang, H., et al. (2020). Distinct responses of Asian summer monsoon to black carbon aerosols and greenhouse gases. *Atmospheric Chemistry and Physics*, *20*(20), 11823–11839. <https://doi.org/10.5194/acp-20-11823-2020>
- Xie, X., Myhre, G., Shindell, D., Faluvegi, G., Takemura, T., Voulgarakis, A., et al. (2022). Anthropogenic sulfate aerosol pollution in South and East Asia induces increased summer precipitation over arid Central Asia. *Communications Earth & Environment*, *3*(1), 328. <https://doi.org/10.1038/s43247-022-00660-x>
- Xie, X., Wang, H., Liu, X., Li, J., Wang, Z., & Liu, Y. (2016). Distinct effects of anthropogenic aerosols on the East Asian summer monsoon between multidecadal strong and weak monsoon stages. *Journal of Geophysical Research: Atmospheres*, *121*(12), 7026–7040. <https://doi.org/10.1002/2015JD024228>
- Zhang, R., & Delworth, T. L. (2006). Impact of Atlantic multidecadal oscillations on India/Sahel rainfall and Atlantic hurricanes. *Geophysical Research Letters*, *33*(17), L17712. <https://doi.org/10.1029/2006GL026267>
- Zhang, Z., & Li, G. (2022). Uncertainty in the projected changes of Sahel summer rainfall under global warming in CMIP5 and CMIP6 multi-model ensembles. *Climate Dynamics*, *59*(11), 3579–3597. <https://doi.org/10.1007/s00382-022-06284-3>
- Zhao, X., Allen, R. J., Wood, T., & Maycock, A. C. (2020). Tropical belt width proportionately more sensitive to aerosols than greenhouse gases. *Geophysical Research Letters*, *47*(7), e2019GL086425. <https://doi.org/10.1029/2019GL086425>